PHYSICAL REVIEW D **80,** 052005 (2009)

Measurement of $B \to D_s^{(*)} K\pi$ branching fractions

J. Wiechczynski,[27] T. Lesiak,[27,4] H. Aihara,[40] K. Arinstein,[1] V. Aulchenko,[1] A. M. Bakich,[37] V. Balagura,[13] E. Barberio,[21] A. Bay,[18] K. Belous,[12] V. Bhardwaj,[32] A. Bondar,[1] A. Bozek,[27] M. Bračko,[20,14] J. Brodzicka,[8] T. E. Browder,[7] Y. Chao,[26] A. Chen,[24] B. G. Cheon,[6] R. Chistov,[13] I.-S. Cho,[44] Y. Choi,[36] J. Dalseno,[8] M. Dash,[43] A. Drutskoy,[3] S. Eidelman,[1] D. Epifanov,[1] N. Gabyshev,[1] A. Garmash,[1] P. Goldenzweig,[3] H. Ha,[16] B.-Y. Han,[16] Y. Hoshi,[39] W.-S. Hou,[26] H. J. Hyun,[17] T. Iijima,[22] K. Inami,[22] A. Ishikawa,[33] M. Iwasaki,[40] D. H. Kah,[17] J. H. Kang,[44] P. Kapusta,[27] H. Kawai,[2] T. Kawasaki,[29] H. Kichimi,[8] H. O. Kim,[17] J. H. Kim,[36] Y. I. Kim,[17] Y. J. Kim,[5] B. R. Ko,[16] P. Križan,[19,14] P. Krokovny,[1] A. Kuzmin,[1] Y.-J. Kwon,[44] S.-H. Kyeong,[44] S. E. Lee,[35] C. Liu,[34] Y. Liu,[22] D. Liventsev,[13] R. Louvot,[18] A. Matyja,[27] S. McOnie,[37] T. Medvedeva,[13] H. Miyata,[29] Y. Miyazaki,[22] T. Mori,[22] Y. Nagasaka,[9] E. Nakano,[31] M. Nakao,[8] H. Nakazawa,[24] K. Nishimura,[7] O. Nitoh,[42] S. Ogawa,[38] T. Ohshima,[22] S. Okuno,[15] H. Ozaki,[8] P. Pakhlov,[13] G. Pakhlova,[13] H. Palka,[27] C. W. Park,[36] H. K. Park,[17] K. S. Park,[36] R. Pestotnik,[14] L. E. Piilonen,[43] A. Poluektov,[1] H. Sahoo,[7] Y. Sakai,[8] O. Schneider,[18] C. Schwanda,[11] A. Sekiya,[23] K. Senyo,[22] M. E. Sevior,[21] M. Shapkin,[12] V. Shebalin,[1] J.-G. Shiu,[26] B. Shwartz,[1] J. B. Singh,[32] A. Sokolov,[12] S. Stanič,[30] M. Starič,[14] J. Stypula,[27] T. Sumiyoshi,[41] G. N. Taylor,[21] Y. Teramoto,[31] I. Tikhomirov,[13] S. Uehara,[8] K. Ueno,[26] T. Uglov,[13] Y. Unno,[6] S. Uno,[8] Y. Usov,[1] G. Varner,[7] K. E. Varvell,[37] K. Vervink,[18] A. Vinokurova,[1] C. H. Wang,[25] M.-Z. Wang,[26] P. Wang,[10] Y. Watanabe,[15] E. Won,[16] B. D. Yabsley,[37] Y. Yamashita,[28] V. Zhilich,[1] V. Zhulanov,[1] T. Zivko,[14] A. Zupanc,[14] N. Zwahlen,[18] and O. Zyukova[1]

(Belle Collaboration)

[1]*Budker Institute of Nuclear Physics, Novosibirsk*
[2]*Chiba University, Chiba*
[3]*University of Cincinnati, Cincinnati, Ohio 45221*
[4]*T. Kościuszko Cracow University of Technology, Krakow*
[5]*The Graduate University for Advanced Studies, Hayama*
[6]*Hanyang University, Seoul*
[7]*University of Hawaii, Honolulu, Hawaii 96822*
[8]*High Energy Accelerator Research Organization (KEK), Tsukuba*
[9]*Hiroshima Institute of Technology, Hiroshima*
[10]*Institute of High Energy Physics, Chinese Academy of Sciences, Beijing*
[11]*Institute of High Energy Physics, Vienna*
[12]*Institute of High Energy Physics, Protvino*
[13]*Institute for Theoretical and Experimental Physics, Moscow*
[14]*J. Stefan Institute, Ljubljana*
[15]*Kanagawa University, Yokohama*
[16]*Korea University, Seoul*
[17]*Kyungpook National University, Taegu*
[18]*École Polytechnique Fédérale de Lausanne (EPFL), Lausanne*
[19]*Faculty of Mathematics and Physics, University of Ljubljana, Ljubljana*
[20]*University of Maribor, Maribor*
[21]*University of Melbourne, School of Physics, Victoria 3010*
[22]*Nagoya University, Nagoya*
[23]*Nara Women's University, Nara*
[24]*National Central University, Chung-li*
[25]*National United University, Miao Li*
[26]*Department of Physics, National Taiwan University, Taipei*
[27]*H. Niewodniczanski Institute of Nuclear Physics, Krakow*
[28]*Nippon Dental University, Niigata*
[29]*Niigata University, Niigata*
[30]*University of Nova Gorica, Nova Gorica*
[31]*Osaka City University, Osaka*
[32]*Panjab University, Chandigarh*
[33]*Saga University, Saga*
[34]*University of Science and Technology of China, Hefei*
[35]*Seoul National University, Seoul*
[36]*Sungkyunkwan University, Suwon*
[37]*University of Sydney, Sydney, New South Wales*

[38]*Toho University, Funabashi*
[39]*Tohoku Gakuin University, Tagajo*
[40]*Department of Physics, University of Tokyo, Tokyo*
[41]*Tokyo Metropolitan University, Tokyo*
[42]*Tokyo University of Agriculture and Technology, Tokyo*
[43]*IPNAS, Virginia Polytechnic Institute and State University, Blacksburg, Virginia 24061*
[44]*Yonsei University, Seoul*
(Received 30 March 2009; published 17 September 2009)

We report a measurement of the exclusive B^+ meson decay to the $D_s^{(*)-}K^+\pi^+$ final state using $657\times 10^6 B\bar{B}$ pairs collected at the $\Upsilon(4S)$ resonance with the Belle detector at the KEKB asymmetric-energy e^+e^- collider. We use $D_s^{*-}\to D_s^-\gamma$ and the $D_s^-\to\phi\pi^-$, $\bar{K}^*(892)^0K^-$ and $K_S^0K^-$ decay modes for $D_s^{(*)}$ reconstruction and measure the following branching fractions: $\mathcal{B}(B^+\to D_s^-K^+\pi^+) = (1.71^{+0.08}_{-0.07}(\text{stat})^{+0.20}_{-0.20}(\text{syst})\pm 0.15(\mathcal{B}_{\text{int}}))\times 10^{-4}$ and $\mathcal{B}(B^+\to D_s^{*-}K^+\pi^+) = (1.31^{+0.13}_{-0.12}(\text{stat})^{+0.25}_{-0.25}(\text{syst})\pm 0.12(\mathcal{B}_{\text{int}}))\times 10^{-4}$. The uncertainties are due to statistics, experimental systematic errors, and uncertainties of intermediate branching fractions, respectively.

DOI: 10.1103/PhysRevD.80.052005 PACS numbers: 13.25.Hw, 14.40.Nd

The dominant process in the decays $B^+\to D_s^{(*)-}K^+\pi^+$ [1] is mediated by the $b\to c$ quark transition and includes the production of an additional $s\bar{s}$ pair, as shown by the Feynman diagram in Fig. 1(a). This process produces at least three final-state particles and can thus be distinguished from much more dominant decays, which include direct D_s production from the W boson vertex. An example of a process that does not involve $s\bar{s}$ quark popping is shown in Fig. 1(b); this is the dominant Feynman diagram describing two-body $B^+\to D_s^{(*)+}\bar{D}^0$ decays with $\bar{D}^0\to K^+\pi^-$. Although both $B^+\to D_s^{(*)-}K^+\pi^+$ and $B^+\to D_s^{(*)+}\bar{D}^0(\bar{D}^0\to K^+\pi^-)$ decays give a similar three-body final state, the different decay mechanisms lead to opposite charges for the D_s and π mesons. In addition, due to the similarities of the final states, the latter decay, $B^+\to D_s^{(*)+}\bar{D}^0$, can be used to check the experimental procedure for the exclusive measurements of the former one, $B^+\to D_s^{(*)-}K^+\pi^+$. These three-body decay modes were recently observed by *BABAR* [2] and need further confirmation.

Studies of $B^+\to D_s^{(*)-}K^+\pi^+$ decays are also motivated by interest in the intermediate resonances that can be formed from the three final-state particles. These resonances are visible as bands in the Dalitz plots for different two-body subsystems [3].

In this paper we report measurements of the branching fractions for $B^+\to D_s^{(*)-}K^+\pi^+$ decays. We also studied the invariant mass distributions for the two-body subsystems to search for new resonances. The analysis is performed on a data sample containing $(657\pm 9)\times 10^6 B\bar{B}$ pairs, collected with the Belle detector at the KEKB asymmetric-energy e^+e^- collider [4] that operates at the $\Upsilon(4S)$ resonance. The production of B^+B^- and $B^0\bar{B}^0$ pairs is assumed to be equal.

The Belle detector is a large-solid-angle magnetic spectrometer that consists of a silicon vertex detector, a 50-layer central drift chamber (CDC), an array of aerogel threshold Cherenkov counters (ACC), a barrel-like arrangement of time-of-flight (TOF) scintillation counters, and an electromagnetic calorimeter composed of CsI(Tl) crystals, located inside a superconducting solenoid coil that provides a 1.5 T magnetic field. An iron flux return located outside of the coil is instrumented to detect K_L^0 mesons and to identify muons. The detector is described in detail elsewhere [5]. Two inner detector configurations were used. A 2.0 cm beam pipe and a 3-layer silicon vertex detector were used for the first sample of $152\times 10^6 B\bar{B}$ pairs, while a 1.5 cm beam pipe, a 4-layer silicon detector, and a small-cell inner drift chamber were used to record the remaining $505\times 10^6 B\bar{B}$ pairs [6].

Charged tracks are required to have a distance of the closest approach to the interaction point less than 5 cm in the beam direction (along the z axis) and less than 5 mm in the transverse $(r-\phi)$ plane. In addition, we only select charged tracks that have transverse momenta larger than 100 MeV$/c$.

To identify charged hadrons, we combine information from the CDC, ACC, and TOF into pion, kaon, and proton likelihood variables $\mathcal{L}_\pi$, $\mathcal{L}_K$, and $\mathcal{L}_p$. For kaon candidates we then require the likelihood ratio $\mathcal{L}_{K/\pi}=\frac{\mathcal{L}_K}{\mathcal{L}_K+\mathcal{L}_\pi}$ to be larger than 0.6. We also apply the proton veto condition $\mathcal{L}_{p/K}<0.95$. Pions are selected from tracks with low kaon probabilities satisfying a likelihood ratio condition $\mathcal{L}_{K/\pi}<0.6$ together with a proton veto $\mathcal{L}_{p/K}<0.95$. In addition, we reject all charged tracks consistent with the electron or muon hypothesis. The above selection results in a typical kaon (pion) identification efficiency ranging from 92% to 97% (94% to 98%) for various decay modes, while 2% to 15% of kaon candidates are misidentified pions and 4% to 8% of pion candidates are misidentified kaons.

The D_s^+ candidates are reconstructed in three final states: $\phi(\to K^+K^-)\pi^+$, $\bar{K}^*(892)^0(\to K^-\pi^+)K^+$, and $K_S^0(\to\pi^+\pi^-)K^+$. We accept K^+K^- $(K^-\pi^+)$ pairs as ϕ $[\bar{K}^*(892)^0]$ candidates if their invariant mass is within 10 (100) MeV$/c^2$ of the nominal ϕ $(\bar{K}^*(892)^0)$ mass [7]. This requirement corresponds to $\pm 2.5\sigma$ in all cases. Candidate

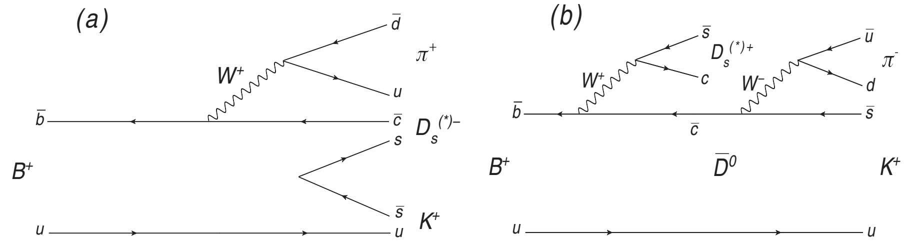

FIG. 1. Diagrams for the decays (a) $B^+ \to D_s^{(*)-} K^+ \pi^+$ and (b) $B^+ \to D_s^{(*)+} \bar{D}^0$, $\bar{D}^0 \to K^+ \pi^-$.

K_S^0 mesons are selected by combining oppositely charged pions with an invariant mass not differing by more than 6 MeV$/c^2$ from the nominal K_S^0 mass. In addition, the vertices of these $\pi^+\pi^-$ pairs must be displaced from the interaction point by at least 5 mm. Photons used for $D_s^* \to D_s \gamma$ reconstruction are accepted if their energies exceed 100 MeV in the laboratory frame. No selection requirements are imposed on the $D_s^{(*)}$ mass at this stage.

A B meson is reconstructed by combining the $D_s^{(*)}$ candidate with an identified kaon and pion and by applying a loose requirement on the quality of the vertex fit (χ_B^2/no. dof < 60) to the K, π, and $D_s^{(*)}$ trajectories, where the $D_s^{(*)}$ mass is constrained to the world average value [7]. The signal B meson decays are identified by three kinematic variables: the $D_s^{(*)}$ invariant mass, the energy difference $\Delta E = E_B - E_{\text{beam}}$, and the beam-energy-constrained mass $M_{\text{bc}} = \sqrt{E_{\text{beam}}^2 - p_B^2}$. Here E_B and p_B are the reconstructed energy and momentum of the B candidate, and E_{beam} is the run-dependent beam energy; all are calculated in the center-of-mass (c.m.) frame. For further analysis we retain events in the candidate region defined as $1.91\ \text{GeV}/c^2 < M(D_s) < 2.03\ \text{GeV}/c^2$ [$2.06\ \text{GeV}/c^2 < M(D_s^*) < 2.16\ \text{GeV}/c^2$], $5.2\ \text{GeV}/c^2 < M_{\text{bc}} < 5.3\ \text{GeV}/c^2$, and $-0.08\ \text{GeV} < \Delta E < 0.2$ GeV. The lower bound in ΔE for candidate events is chosen to exclude a possible background from $B \to D_s X$ decays with higher multiplicities. From GEANT [8] based Monte Carlo (MC) simulation, we deduce that the signal peaks in a signal region defined by the requirements: $1.9532\ \text{GeV}/c^2 < M(D_s) < 1.9832\ \text{GeV}/c^2$ [$2.092\ \text{GeV}/c^2 < M(D_s^*) < 2.132\ \text{GeV}/c^2$], $5.27\ \text{GeV}/c^2 < M_{\text{bc}} < 5.29\ \text{GeV}/c^2$, and $|\Delta E| < 0.03$ GeV. Based on MC simulation, the region $2.88\ \text{GeV}/c^2 < M(K^+K^-\pi^+\pi^-) < 3.18\ \text{GeV}/c^2$ is excluded to remove background from $B^+ \to ((c\bar{c}) \to K^+K^-\pi^+\pi^-)K^+$ decays, where $(c\bar{c})$ are charmonium states such as the J/ψ or η_c. For $B^+ \to D_s^+ \bar{D}^0 (\to K^+\pi^-)$ decays the events in the candidate region are required to have $K^+\pi^-$ invariant mass within a 15 MeV$/c^2$ (3σ) interval of the nominal D^0 mass.

We find that for $B^+ \to D_s^- K^+ \pi^+$ ($B^+ \to D_s^{*-} K^+ \pi^+$) decays at most 11% (29%) of events have more than one B candidate. In such cases we select the B candidate with the smallest value of χ_B^2. Moreover, when there are at least two combinations with the same χ_B^2 value, the one containing a kaon—originating directly from the B decay—with the highest likelihood ratio $\mathcal{L}_{K/\pi}$ is selected. For $B \to D_s^* K\pi$ decays, we further choose the combination that minimizes the quantity $|M(D_s^*) - M(D_s) - 143.8\ \text{MeV}/c^2|$.

We exploit the event topology to discriminate between spherical $B\bar{B}$ events and the dominant background from jetlike continuum events, $e^+e^- \to q\bar{q}$ ($q = u, d, s, c$). We use the event shape variable R_2 defined as the ratio of the second and zeroth Fox-Wolfram moments [9] and require that R_2 be less than 0.4.

The signal yields are extracted using unbinned extended maximum-likelihood fits to the (ΔE, M_{bc}, $M(D_s^{(*)})$) distributions of the selected candidate events. The likelihood function is given by

$$\mathcal{L} = \frac{1}{N!}(N_S + N_B)^N e^{-N_S - N_B} \times \prod_{i=1}^{N} \left(\frac{N_S}{N_S + N_B} \mathcal{P}_S^i + \frac{N_B}{N_S + N_B} \mathcal{P}_B^i \right), \tag{1}$$

where i is the event identifier, N is the total number of events in the fit, and $N_S(N_B)$ is the number of signal and background events, respectively. We use Gaussian functions to parametrize the signal probability density function in ΔE and M_{bc} and a double Gaussian function with a common mean for the $M(D_s^{(*)})$ distribution:

$$\begin{aligned}\mathcal{P}_S^i = {}& \mathcal{G}(\Delta E^i; \overline{\Delta E}, \sigma_{\Delta E}) \mathcal{G}(M_{\text{bc}}^i; m_B, \sigma_{M_{\text{bc}}}) \\ & \times [f_{D_s^{(*)}}^S \mathcal{G}(M^i(D_s^{(*)}); m_{D_s^{(*)}}, \sigma_{D_s^{(*)}}^{(1)}) \\ & + (1 - f_{D_s^{(*)}}^S) \mathcal{G}(M^i(D_s^{(*)}); m_{D_s^{(*)}}, \sigma_{D_s^{(*)}}^{(2)})],\end{aligned} \tag{2}$$

where $\overline{\Delta E}$, m_B, $m_{D_s^{(*)}}$, $\sigma_{\Delta E}$, $\sigma_{M_{\text{bc}}}$, $f_{D_s^{(*)}}^S$, $\sigma_{D_s^{(*)}}^{(1)}$, and $\sigma_{D_s^{(*)}}^{(2)}$ are fit parameters. The latter three, which describe the signal shape corresponding to the $M(D_s^{(*)})$ distributions, are fixed to the values obtained from the fit to the $B^+ \to D_s^{(*)+} \bar{D}^0$ control channels. In addition, we use the $B^+ \to D_s^{*+} \bar{D}^0$ data samples to fix the signal widths for ΔE and M_{bc} for the $B^+ \to D_s^{*-} K^+ \pi^+$ decays.

The background is parametrized with a second-order polynomial (p_2) in the ΔE distribution. For the M_{bc} background distribution we choose a parametrization that was first used by the ARGUS Collaboration [10], $f(M_{\rm bc}, \zeta) \propto M_{\rm bc}\sqrt{1-(M_{\rm bc}/E_{\rm beam})^2}e^{-\zeta(1-(M_{\rm bc}/E_{\rm beam})^2)}$, where ζ is a fit parameter. Finally, the $M(D_s^{(*)})$ background distribution is described by the sum of a double Gaussian function and a second-order polynomial:

$$\begin{aligned}\mathcal{P}_B^i = {}& p_2(\Delta E^i; w_0, w_1, w_2) f(M_{\rm bc}^i; \zeta) \\ & \times [p_2(M^i(D_s^{(*)}); v_0, v_1, v_2) \\ & + f^B_{D_s^{(*)}} \mathcal{G}(M^i(D_s^{(*)}); m_{D_s^{(*)}}, \sigma^{(1)}_{D_s^{(*)}}) \\ & + (1 - f^B_{D_s^{(*)}}) \mathcal{G}(M^i(D_s^{(*)}); m_{D_s^{(*)}}, \sigma^{(2)}_{D_s^{(*)}})]. \end{aligned} \quad (3)$$

The values of the variables w_0, w_1, w_2, ζ, v_0, v_1, and v_2 are determined in the fit, whereas the $f^B_{D_s^{(*)}}$ are fixed to the values resulting from the fits to the appropriate control channels. Figures 2 and 3 show the distributions of ΔE, $M_{\rm bc}$, and $M(D_s^{(*)})$ together with the fits described above.

For decays containing a $K^*(892)^0$ meson a few percent correction is applied to the signal yields obtained from the fit. The $K^*(892)^0$ mass sidebands, (0.746–0.796) GeV$/c^2$ and (0.996–1.046) GeV$/c^2$, are fitted and a noticeable background contributing to the signal yields is found for the $B^+ \to D_s^-(\to K^{*0}K^-)K^+\pi^+$ and $B^+ \to D_s^+(\to K^{*0}K^-)\bar{D}^0$ channels. Final signal yields are ob-

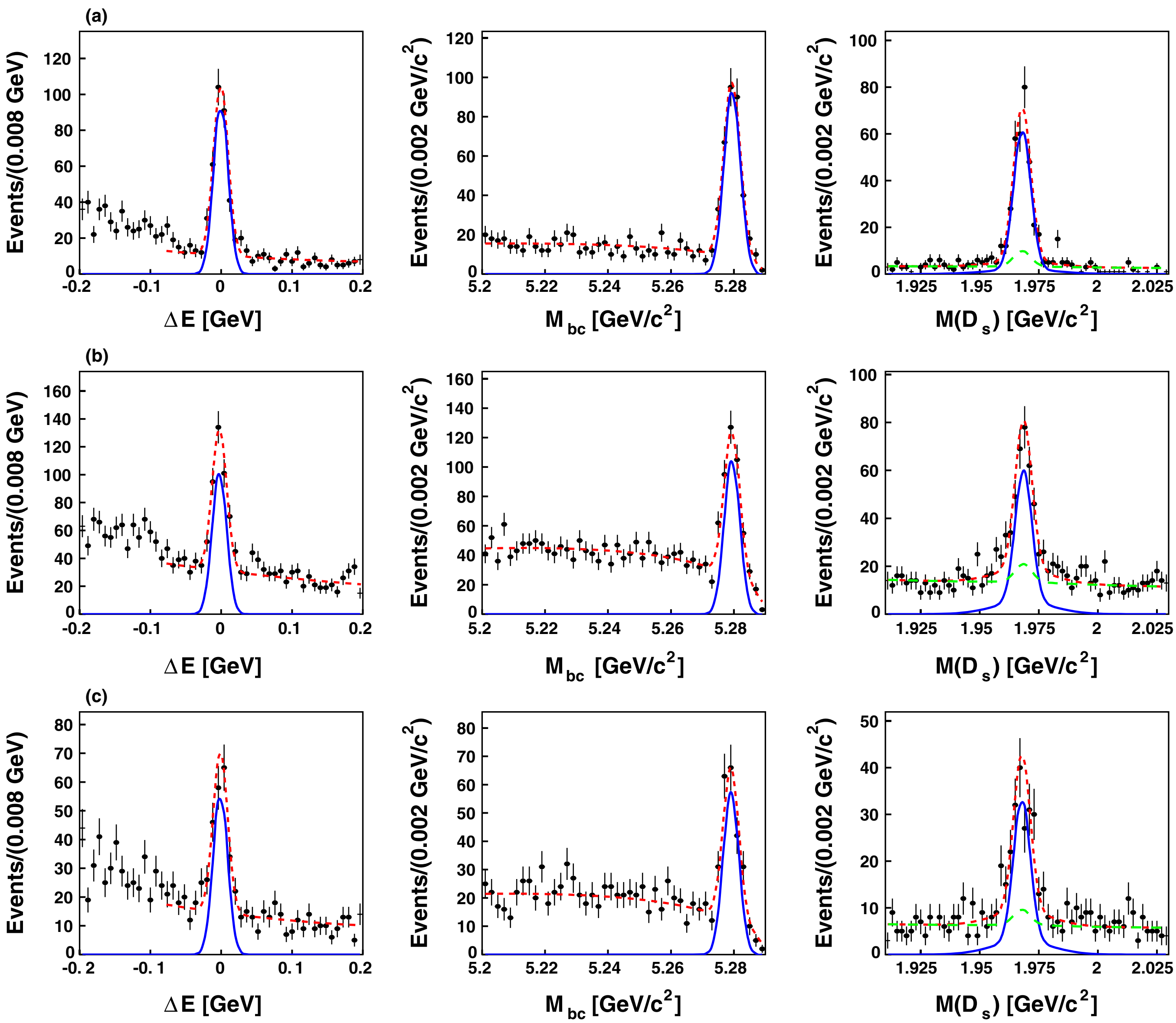

FIG. 2 (color online). Distributions of ΔE, $M_{\rm bc}$, and $M(D_s)$ for (a) $B^+ \to D_s^-(\to \phi\pi^-)K^+\pi^+$, (b) $B^+ \to D_s^-(\to K^{*0}K^-)K^+\pi^+$, and (c) $B^+ \to D_s^-(\to K_S^0K^-)K^+\pi^+$ decays. The distribution for each quantity—ΔE, $M_{\rm bc}$, and $M(D_s)$—is shown in the signal region of the remaining two quantities. The red dashed curves show the results of the overall fit described in the text, the blue solid curves correspond to the signal components, and the green long-dashed curves indicate the fitted background for $M(D_s)$.

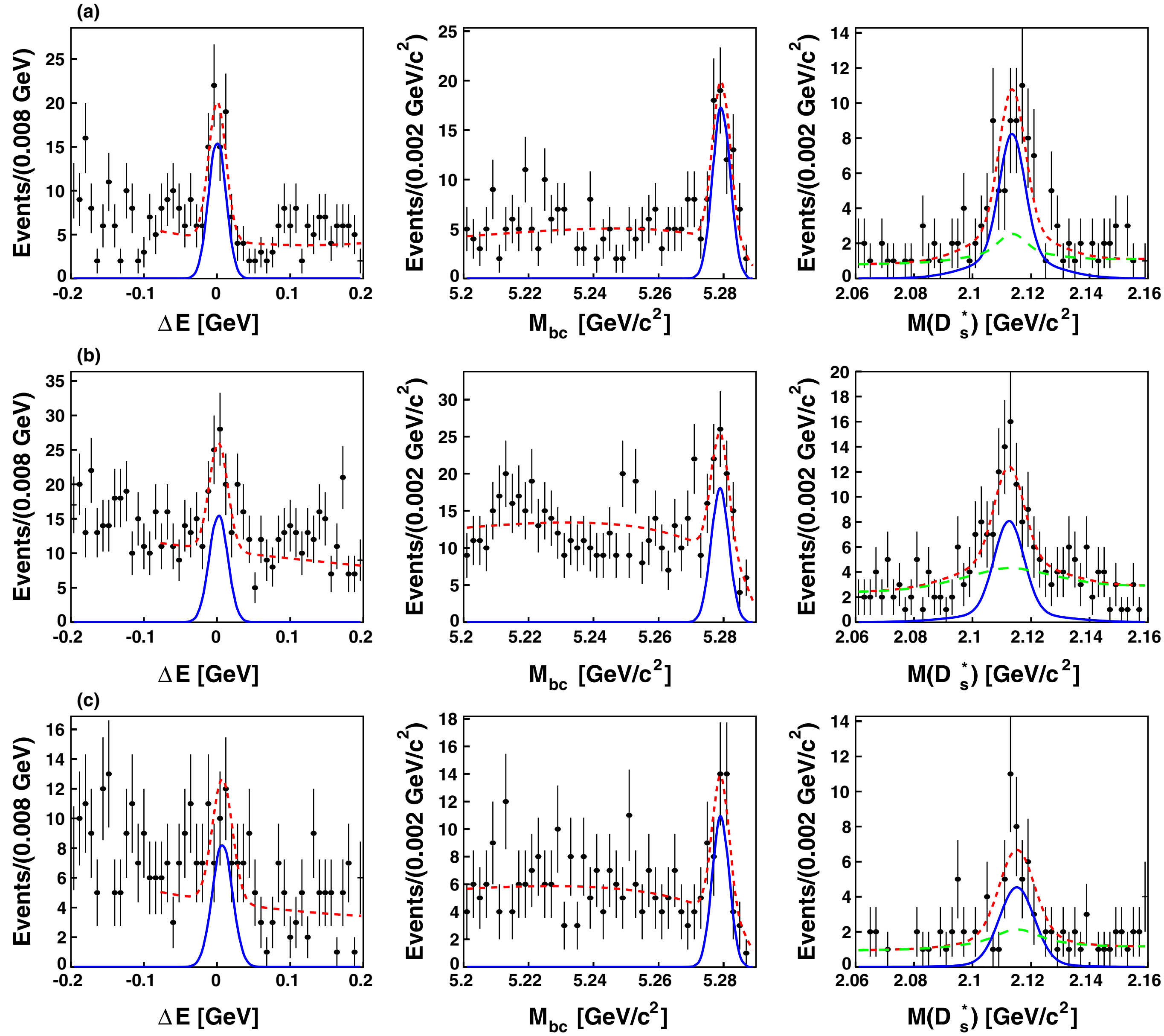

FIG. 3 (color online). Distributions of ΔE, $M_{\rm bc}$, and $M(D_s^*)$ for (a) $B^+ \to D_s^{*-}(\to \phi\pi^-)K^+\pi^+$, (b) $B^+ \to D_s^{*-}(\to K^{*0}K^-)K^+\pi^+$, and (c) $B^+ \to D_s^{*-}(\to K_S^0K^-)K^+\pi^+$ decays. The distribution for each quantity—ΔE, $M_{\rm bc}$, and $M(D_s^*)$—is shown in the signal region of the remaining two quantities. The red dashed curves show the results of the overall fit described in the text, the blue solid curves correspond to the signal components, and the green long-dashed curves indicate the fitted background for $M(D_s^*)$.

tained by subtracting these contributions from the nominal fit values.

The signal yields together with statistical significances are listed in Table I. The significance is defined as $\sqrt{-2\ln(\mathcal{L}_0/\mathcal{L}_{\rm max})}$, where $\mathcal{L}_{\rm max}$ ($\mathcal{L}_0$) denotes the maximum likelihood with the signal yield at its nominal value (fixed to zero).

The reconstruction efficiencies, determined using MC samples of $e^+e^- \to \Upsilon(4S) \to B^+B^-$ decays, are listed in Table I. This table also contains the values obtained for the branching fractions of the decays $B^+ \to D_s^{(*)-}K^+\pi^+$ and $B^+ \to D_s^{(*)+}\bar{D}^0$. The last error (Table I) is due to uncertainties in the branching fractions for the decays of intermediate particles, predominantly those of the $D_s^{(*)}$ [7]. The systematic uncertainties are evaluated only for the three-body $B^+ \to D_s^{(*)-}K^+\pi^+$ decays. We find branching fractions for the $B^+ \to D_s^{(*)+}\bar{D}^0$ control samples in agreement with world averages [7].

Systematic uncertainties are listed in Table II. The contribution (f) due to the selection procedure is dominated by the R_2 requirement. This uncertainty is estimated conservatively as the maximum variation of the efficiency-

TABLE I. Signal yields, reconstruction efficiencies, statistical significances, and branching fractions for $B^+ \to D_s^{(*)-} K^+ \pi^+$ and $B^+ \to D_s^{(*)+} K^+ \pi^-$ decays.

Decay	Signal yield	Efficiency (%)	Statistical signif. (σ)	Branching fraction (10^{-4})
$B^+ \to D_s^- (\to \phi\pi^-) K^+ \pi^+$	$306.0^{+19.7}_{-19.1}$	13.09 ± 1.00	31.5	$1.63^{+0.11+0.18}_{-0.10-0.18} \pm 0.25$
$B^+ \to D_s^- (\to K^{*0} K^-) K^+ \pi^+$	$281.7^{+24.7}_{-23.6}$	9.48 ± 0.67	26.5	$1.74^{+0.15+0.20}_{-0.15-0.20} \pm 0.27$
$B^+ \to D_s^- (\to K_S^0 K^-) K^+ \pi^+$	$179.4^{+16.7}_{-16.0}$	14.49 ± 1.11	20.4	$1.82^{+0.17+0.24}_{-0.16-0.25} \pm 0.11$
$B^+ \to D_s^{*-} (\to \phi\pi^-) K^+ \pi^+$	$59.0^{+9.3}_{-8.6}$	3.51 ± 0.52	11.0	$1.24^{+0.20+0.23}_{-0.18-0.23} \pm 0.19$
$B^+ \to D_s^{*-} (\to K^{*0} K^-) K^+ \pi^+$	$61.7^{+10.6}_{-9.8}$	2.88 ± 0.42	9.3	$1.33^{+0.23+0.25}_{-0.21-0.25} \pm 0.21$
$B^+ \to D_s^{*-} (\to K_S^0 K^-) K^+ \pi^+$	$35.7^{+7.7}_{-6.9}$	4.02 ± 0.59	8.0	$1.39^{+0.30+0.29}_{-0.27-0.28} \pm 0.08$
$B^+ \to D_s^+ (\to \phi\pi^+) \bar{D}^0$	$597.4^{+25.0}_{-24.3}$	13.03 ± 0.12	56.8	$82.31^{+3.45}_{-3.35} \pm 12.50$
$B^+ \to D_s^+ (\to \bar{K}^{*0} K^+) \bar{D}^0$	$512.6^{+26.2}_{-25.3}$	9.21 ± 0.10	53.3	$83.80^{+4.28}_{-4.14} \pm 12.94$
$B^+ \to D_s^+ (\to K_S^0 K^+) \bar{D}^0$	$294.5^{+17.8}_{-17.2}$	14.22 ± 0.20	38.9	$78.61^{+4.74}_{-4.56} \pm 4.86$
$B^+ \to D_s^{*+} (\to \phi\pi^+) \bar{D}^0$	$150.2^{+15.7}_{-14.8}$	3.97 ± 0.07	19.0	$72.15^{+7.52}_{-7.12} \pm 10.98$
$B^+ \to D_s^{*+} (\to \bar{K}^{*0} K^+) \bar{D}^0$	$151.9^{+15.1}_{-14.3}$	3.09 ± 0.06	20.8	$78.68^{+7.83}_{-7.43} \pm 12.16$
$B^+ \to D_s^{*+} (\to K_S^0 K^+) \bar{D}^0$	$95.3^{+12.4}_{-11.6}$	4.40 ± 0.12	15.0	$87.27^{+11.32}_{-10.63} \pm 5.43$

corrected signal yield, when the R_2 selection value is varied over a wide range (values between 0.25 and 0.55). The uncertainty (g) due to the fit range is determined by varying the candidate region. To evaluate the contribution (h) we repeat the fits varying the shape parameters by $\pm 1\sigma$. The uncertainty (i) is estimated as the statistical error in the selection efficiency, increased conservatively by a factor obtained from the difference between the value of the branching fraction for the appropriate control channel and the generated branching fraction. The systematic uncertainty (i) also includes efficiency variations over the $M(D_s^{(*)}K)$ phase space. The overall systematic error is obtained by summing these contributions in quadrature.

The average branching fractions for the decays $B^+ \to D_s^- K^+ \pi^+$ and $B^+ \to D_s^{*-} K^+ \pi^+$ are determined from a simultaneous fit to the data containing events from all three D_s decay modes. Here, the systematic uncertainties are calculated as in the individual channels (Table II).

In summary, the following branching fractions are determined:

$$\mathcal{B}(B^+ \to D_s^- K^+ \pi^+) = (1.71^{+0.08}_{-0.07}(\text{stat})^{+0.20}_{-0.20}(\text{syst}) \pm 0.15(\mathcal{B}_{\text{int}})) \times 10^{-4}, \quad (4)$$

$$\mathcal{B}(B^+ \to D_s^{*-} K^+ \pi^+) = (1.31^{+0.13}_{-0.12}(\text{stat})^{+0.25}_{-0.25}(\text{syst}) \pm 0.12(\mathcal{B}_{\text{int}})) \times 10^{-4}. \quad (5)$$

These branching fractions are compatible with the values reported by the *BABAR* Collaboration [2].

The invariant mass distributions of the $D_s^{(*)-} K^+$ subsystem are incompatible with those expected for three-body phase space production and exhibit strong enhancements around 2.7 GeV$/c^2$ (see Fig. 4). These features may be

TABLE II. Systematic uncertainties on the branching fractions for $B^+ \to D_s^{(*)-} K^+ \pi^+$ decay modes, given in percent.

Source	D_s^- final state $\phi\pi^-$	D_s^- final state $K^{*0}K^-$	D_s^- final state $K_S^0 K^-$	D_s^{*-} final state $\phi\pi^-\gamma$	D_s^{*-} final state $K^{*0}K^-\gamma$	D_s^{*-} final state $K_S^0 K^-\gamma$
(a) Tracking	5	5	5	5	5	5
(b) Hadron identification	5	5	5	5	5	5
(c) K_S^0 reconstruction	⋯	⋯	4.5	⋯	⋯	4.5
(d) Photon reconstruction	⋯	⋯	⋯	5	5	5
(e) Uncertainty in $N(B\bar{B})$	1.4	1.4	1.4	1.4	1.4	1.4
(f) Selection procedure	3.7	3.7	3.7	3.7	3.7	3.7
(g) Size of candidate region	0.6	1.1	1.1	0.3	0.2	1.5
(h) Signal shape	$^{+1.2}_{-1.3}$	$^{+3.4}_{-3.4}$	$^{+5.6}_{-6.3}$	$^{+5.6}_{-6.7}$	$^{+6.9}_{-7.4}$	$^{+9.7}_{-7.8}$
(i) MC statistics	7.6	7.0	7.7	14.8	14.5	14.8
Total	$^{+11.2}_{-11.2}$	$^{+11.3}_{-11.3}$	$^{+13.3}_{-13.6}$	$^{+18.5}_{-18.8}$	$^{+18.6}_{-18.9}$	$^{+20.7}_{-19.8}$

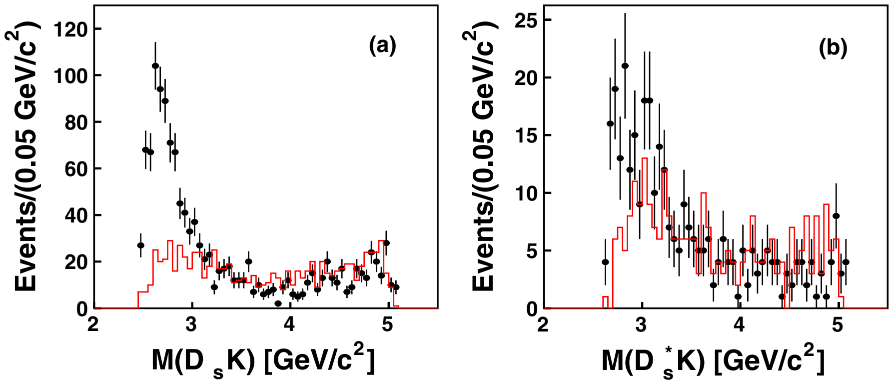

FIG. 4 (color online). The invariant mass distributions of (a) $D_s^- K^+$ for the decay $B^+ \to D_s^- K^+ \pi^+$ and (b) of $D_s^{*-} K^+$ for $B^+ \to D_s^{*-} K^+ \pi^+$ corresponding to the signal regions described in the text. The histograms show the background contributions corresponding to 5.22 GeV $< M_{bc} <$ 5.24 GeV.

explained by the production of charm resonances with masses below $D_s^{(*)-} K^+$ threshold [3]. The discrepancy between the data sample and the MC phase space distribution is taken into account in evaluation of the efficiency and the corresponding systematic uncertainty.

We thank the KEKB group for the excellent operation of the accelerator, the KEK cryogenics group for the efficient operation of the solenoid, and the KEK computer group and the National Institute of Informatics for valuable computing and SINET3 network support. We acknowledge support from the Ministry of Education, Culture, Sports, Science, and Technology (MEXT) of Japan, the Japan Society for the Promotion of Science (JSPS), and the Tau-Lepton Physics Research Center of Nagoya University; the Australian Research Council and the Australian Department of Industry, Innovation, Science and Research; the National Natural Science Foundation of China under Contracts No. 10575109, No. 10775142, No. 10875115, and No. 10825524; the Department of Science and Technology of India; the BK21 program of the Ministry of Education of Korea, the CHEP src program and Basic Research program (Grant No. R01-2008-000-10477-0) of the Korea Science and Engineering Foundation; the Polish Ministry of Science and Higher Education; the Ministry of Education and Science of the Russian Federation and the Russian Federal Agency for Atomic Energy; the Slovenian Research Agency; the Swiss National Science Foundation; the National Science Council and the Ministry of Education of Taiwan; and the U.S. Department of Energy. This work is supported by a Grant-in-Aid from MEXT for Science Research in a Priority Area (''New Development of Flavor Physics''), and from JSPS for Creative Scientific Research (''Evolution of Tau-lepton Physics'').

[1] Throughout this paper, the inclusion of the charge-conjugate decay mode is implied unless otherwise stated.
[2] B. Aubert *et al.* (*BABAR* Collaboration), Phys. Rev. Lett. **100**, 171803 (2008).
[3] O. Antipin and G. Valencia, Phys. Lett. B **647**, 164 (2007).
[4] S. Kurokawa and E. Kikutani, Nucl. Instrum. Methods Phys. Res., Sect. A **499**, 1 (2003), and other papers included in this volume.
[5] A. Abashian *et al.* (Belle Collaboration), Nucl. Instrum. Methods Phys. Res., Sect. A **479**, 117 (2002).
[6] Z. Natkaniec *et al.* (Belle SVD2 Group), Nucl. Instrum. Methods Phys. Res., Sect. A **560**, 1 (2006).
[7] C. Amsler *et al.*, Phys. Lett. B **667**, 1 (2008).
[8] R. Brun *et al.*, GEANT 3.21, CERN Report No. DD/EE/84-1, 1984.
[9] G. C. Fox and S. Wolfram, Phys. Rev. Lett. **41**, 1581 (1978).
[10] H. Albrecht *et al.* (ARGUS Collaboration), Phys. Lett. B **241**, 278 (1990).